

Two-dimensional soot distributions in buoyant turbulent fires

Yibing Xin*, Jay P. Gore

School of Mechanical Engineering, Purdue University, West Lafayette, IN 47906, USA

Abstract

Spatially resolved two-dimensional soot volume fractions were measured using laser-induced incandescence in 7.1 cm methane and ethylene turbulent buoyant flames to study the distributions of soot in vertical and horizontal planes, and to provide data for soot model validation. Factors affecting the LII signals were considered including the laser energy profile and the laser attenuation effects. The absolute soot volume fractions were obtained by comparison to existing extinction measurements. The instantaneous soot images were collected to cover the entire flame height. Statistical quantities of soot volume fractions including mean, root mean square, probability density function, and spatial correlation coefficient were calculated at five downstream locations. The results show that instantaneous distributions of soot volume fractions exhibit significant differences compared to the ensemble averages, strong fluctuation around the mean, relatively homogeneous probability density function, and highly anisotropic spatial correlation. © 2004 The Combustion Institute. Published by Elsevier Inc. All rights reserved.

Keywords: Soot; Buoyant turbulent fire; Laser-induced incandescence

1. Introduction

Soot is one of the main pollutants in combustion process and plays a significant role in flame radiation. In fire research, soot is of particular importance because of smoke damage and fire spread as a result of soot dominated radiation. Therefore, knowledge of soot distribution is crucial to study smoke and radiation in turbulent fires. From the past work of Hamins et al. [1,2] and Klassen et al. [3–5], it has been recognized that:

- (1) If time series of soot volume fractions and temperature along the radiation path are available from measurements or predictions, radiation heat flux can be predicted reasonably well.
- (2) Turbulence–radiation interactions are significant. Therefore, predictions of mean soot volume fractions and mean temperatures are not sufficient.
- (3) The emission-based soot volume fraction is lower than the absorption-based soot volume fraction by a large value, which can only be partly explained by consideration of scattering, indicating that a 10 mm long probe volume does not have a homogeneous temperature.
- (4) Effects of spatial correlations are significant in determining the radiation intensity leaving a path. For example simultaneous occurrence of many hot soot streaks along a radiation

* Corresponding author. Present address: FM Global Research, 1151, Boston-Providence Turnpike, Norwood, MA 02062, USA. Fax: +1 781 255 4024.

E-mail address: yibing.xin@fmglobal.com (Y. Xin).

path causes very high instantaneous flux. Therefore, simultaneous line-of-sight and planar measurements of soot volume fractions are necessary.

Motivated by these, soot volume fractions in weakly (methane) and moderately (ethylene) sooty buoyant fires were measured using planar laser-induced incandescence (LII) technique. The aim of this work was to study the spatial distributions of soot in vertical and horizontal planes in turbulent fires and to provide data for development and validation of soot models in large-eddy simulation type code for fires, e.g., the Fire Dynamic Simulator [6,7]. Factors affecting the LII signal, especially the effects of laser energy profile (LEP) and laser attenuation, were considered in the measurements. Calibrations of the LII signals were conducted by comparison to known soot volume fractions of a laminar co-flow ethylene/air flame [8]. The statistical quantities of the soot volume fractions including the ensemble mean, root mean square (RMS), probability density function (PDF), and spatial correlation coefficient (SCC) were calculated using instantaneous soot images. The important features of soot distributions were analyzed to address the questions regarding the differences between instantaneous and mean soot distributions, the fluctuation intensities of the soot volume fractions around the mean, and the homogeneity of the soot in the entire fire flow field.

2. Experimental method

2.1. Facilities and instruments

Schematic arrangement of the LII system is shown in Fig. 1. A 7° diffuser burner made of sheet metal is utilized to establish the buoyant flames with 7.1 cm exit diameter fueled by methane and ethylene, respectively. The diffuser pro-

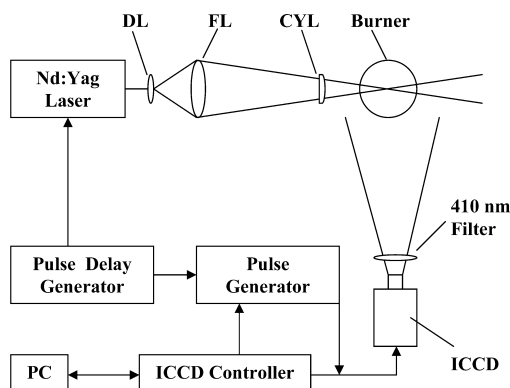


Fig. 1. Plan view of the experimental system.

vides a uniform velocity distribution at the fuel exit surface [9]. Gaseous fuels were particularly selected to avoid the coupling of radiation feedback and fuel evaporation or pyrolysis, which are typical for liquid and solid fires, so that soot models can be independently evaluated. The burner was mounted vertically on a three-dimensional translation system. Commercial grade fuels enter the bottom of the burner and burn in quiescent ambient air. Because the fire is buoyancy-dominated, very weak, and sensitive to even small drafts in the laboratory, all exhaust fans were shut off during the measurements. A double-walled wire-mesh enclosure was used to prevent ambient disturbances. During experimental intervals, room air was changed using exhaust fans to recover the initial conditions.

A Nd:Yag laser (10 Hz repetition rate) was used to heat the soot particle to incandescence. The laser provides energy up to 1.2 J/pulse at 1064 nm. Based on LII theories [10–13], an energy density threshold of 0.4 J/cm² is required to achieve soot incandescence at 1064 nm and 0.2 J/cm² at 532 nm. Therefore, the visible (532 nm) second harmonic of the laser was used in the present work. The energy output of the laser was 420 mJ/pulse (8 ns full width at half maximum). The laser sheet was formed using diverging (DL), focusing (FL), and cylindrical (CYL) lenses (Fig. 1), which created a probe plane with an effective height of 3.5 cm and a thickness of 1 mm through burner axis. The effective thickness of the probe plane determined the spatial resolution of the LII measurement. Considering the energy variation across the laser sheet due to the Gaussian beam profile, only 2.0 cm around the laser axis was actually used in data collection. The mean energy density in the probe plane, calculated based on these parameters, was 150 MW/cm².

The LII signal was collected using an intensified charge couple device (ICCD, Princeton Instrument). The linearity of this device was examined using neutral density filters and a uniform light source. Factors were considered in selecting the detection wavelength including the spectral location of the peak LII signal and interferences resulting from flame emission, laser scattering, laser-induced fluorescence, and chemiluminescence. Different viewpoints exist on how to select the detection strategy [12–15]. The method used in this work is based on the suggestions of [16,17]. A band-pass interference filter with peak transmission wavelength at 410 ± 10 nm was mounted in front of the ICCD to avoid the most common interference sources. The collection of LII signals was delayed by 40 ns using a Pulse Delay Generator (Stanford DG 535) with an intensifier gate width of 35 ns produced by a Pulse Generator (Princeton Instrument FG100).

The spatial resolution of the LII image was determined by the pixel size of the ICCD Mul-

ti-Channel Plate (MCP) and the detection optics. The overall result in the present experiment was that each pixel corresponds to a $0.2\text{ mm} \times 0.2\text{ mm}$ region in the probe plane. To accommodate the data transfer speed through the ICCD controller (4–5 s/frame), repetition rate of the laser (10 Hz), and the pulsation frequency of the pool fire (5–6 Hz), LII images were collected at relatively long time intervals (1 h/700 images). The collection time was randomly selected to avoid phase-lock bias in the data caused by fire puffing. Statistical quantities including the ensemble mean, RMS, PDF, and SCC, therefore, can be calculated using these randomly collected images.

2.2. Experimental conditions

For the methane (BOC Gases, Commercial Grade 1.3, >93%) and ethylene (BOC Gases, Grade 2.5, >99.5%,) flames, the fuel flow rates were 84.3 and 72.8 mg/s, and the visible flame heights 36.4 and 38.8 cm, respectively. The calculated fire Froude number [18] was 0.109 for both cases, which matches that of a 7.1 cm toluene pool fire reported by Zhou and Gore [19]. This essentially preserves the ratio of local buoyancy produced by thermal expansion and the overall buoyancy of the fire flow. Instantaneous LII images of 2 cm high were collected at 20 downstream locations to cover the entire flame height to observe the instantaneous soot distributions. Then, 3500 samples of the soot volume fractions were measured to study the statistics of soot volume fractions at each of the five downstream locations of $H = 1/2D, 1D, 2D, 3D,$ and $4D$, where H is the elevation above the burner exit and D is the burner diameter.

2.3. Corrections and calibration of LII signals

Interference signals of LII are usually caused by laser scattering, laser-induced fluorescence, flame emission, C_2 emission, and chemiluminescence. These signals were either blocked by the bandpass filter or avoided by the time delay of ICCD in this work. However, ICCD MCP spatial response, or flat field effect, and LEP effect cannot be avoided, and thus have to be minimized and corrected by calibration.

The flat field effect is simply the result of variations in pixel response characteristics. To correct this effect, a 2.54 cm diameter blackbody was used as a uniform illumination source to calibrate all the pixels. The normalized flat field image indicates the deviation from the average single level is within 20%. All LII signals were divided by the normalized flat field image prior to any further processing.

The LEP effect is the distortion of LII signal caused by the Gaussian spatial beam profile of

the laser. Although both laser incident intensity and LII attenuation affect the measurements, we tested methane, ethylene, and acetylene flames, and found that the LEP effect was the major factor. Detailed discussion of this effect can be found in [14,20]. In the present work, the distorted signals were corrected using a single point translation method. A single point with a known soot volume fraction in a steady laminar co-flow ethylene/air flame (60 mm downstream along flame axis in [8]) was translated vertically across the laser sheet. The LII signals from this point subjected to various laser energy levels were collected at 1 mm intervals. The results were then normalized and fitted to polynomials to generate the LEP correction curve. Each data point on the LEP correction curve was obtained by averaging 200 samples. In this work, only vertical variation of the laser energy was considered, and each column of pixels on the LII image was divided by this curve to eliminate the LEP effect.

Along the laser propagation path, soot particles absorb the laser energy resulting in an attenuation effect on LII signals. Shaddix and Smyth [13] studied this effect and pointed out that the LII signal is weakly dependent on the laser incident energy for a Gaussian beam profile. In the present work, an estimation of this effect using the measured soot volume fractions and Bouguer's law of extinction indicates that in the sootiest region, 38% of LII images in the methane flame exhibit more than 20% laser attenuation compared to 79% in the ethylene flame. Therefore, the results and discussions of soot distributions in the following sections will be primarily based on the measurements of the methane flame. Samples of measurements in the ethylene flame will be given at the end of this paper to qualitatively examine the fuel effect.

To convert the relative LII signals to absolute soot volume fractions, a calibration procedure was adopted by comparing the LII measurements to previous extinction measurements in a laminar co-flow flame [8]. Experimental conditions of an ethylene/air diffusion flame by Gore and Faeth [8] were duplicated, and the known peak soot volume fraction at an axial distance of 60 mm was used to calibrate the LII signals. It is recognized that there might be significant uncertainties associated with soot optical properties in extinction measurements. But the major portion of the results in this work including soot distribution patterns, fluctuation intensities, PDF, and SCC was not affected.

2.4. Uncertainties and statistical convergence

The sources of experimental uncertainties of instantaneous LII signals are caused by the laser incidence and the detection system. The Nd:Yag laser was warmed up for 30 min to achieve steady

laser energy output. A Silicon PIN Detector (ET-2000, Electro-Optics Technology) was then utilized to monitor the variation of the laser energy output. The results show that the energy fluctuation is within 7%. Compared to this relatively low value, the LEP effect results in 20% deviation. It was also observed that the portion of the co-flow laminar flame used for LII calibration slightly flickers around the mean position. This together with the steep soot gradient near the peak and laser attenuation leads to additional errors in the calibration procedure. The estimated uncertainty associated with the calibration procedure is 11%. In the detection system, the flat field effect exhibits 20% signal correction. The dark current and thermal noise are the basic sources to produce noise in the ICCD. In the present work, the ICCD is water-cooled to $-33\text{ }^{\circ}\text{C}$ so that the detection limits in the methane and ethylene flames are 0.046 and 0.138 ppm, respectively, for the instantaneous images.

Another source of uncertainties is the particle size bias in soot heating and cooling. We made an effort to reduce the influence by minimizing the gate delay time. Theoretically, the local gas temperatures may also affect the LII signal. But this effect was so secondary that it was not observed in both under- and over-fire regions.

The uncertainties associated with the statistical convergence were determined by comparing the averages of two groups of randomly selected LII images among the 3500 samples at each location in the measurements. Each group contains 1400 samples, and the uncertainty was defined as the ratio between the difference of the means of the two groups and the overall mean of the 2800 samples. The results of this analysis show that the standard deviation is less than 24% for a group of 1400 samples. Therefore, we estimated that the standard deviation of the average over 3500 samples is less than 10%. Considering that the LEP effect is dominant in LII uncertainties and the statistical uncertainties are independent, we estimated that the overall uncertainties are 30%.

3. Results and discussions

3.1. Instantaneous soot distributions in the methane flame

A collage of representative instantaneous images of soot volume fractions in the 7.1 cm methane flame is shown in Fig. 2. A thin blank space was left between neighboring stripes to signify that the images were not taken simultaneously. In the entire flame, soot particles are not dispersed uniformly, but in thin regions called streaks, which occupy only a very small fraction of the flame zone. The apparent thickness of these streaks, defined as the full width at half maximum

of soot volume fractions normal to each streak, typically ranges between 1 and 2 mm. In the persistent zone near the burner exit [21], the soot distributions are similar to those in a laminar flame [22], i.e., the soot particles form a conical layer that flickers around the burner axis. Away from this region along the downstream, flame necking and bulging occur so that multiple soot streaks can be seen in the probe plane. In the intermittent and plume zones [21], the soot streaks are wrinkled and twisted by the turbulent flow resulting in highly curved structures in some locations, e.g., $H = 2.5D - 3D$. Preliminary horizontal LII visualization of soot was conducted at $H = 0.5D$ perpendicular to the burner axis with laser traveling from right to left (Fig. 3). Each panel in Fig. 3 is a raw instantaneous LII image without calibration and correction. As a result, the observed laser heated region is much larger than the 2 cm stripes in Fig. 2. This preliminary visualization confirms that soot streaks occupy only a small fraction of the flame zone. Taking Figs. 2 and 3 together, we believe that soot distributions in this buoyant fire are essentially two-dimensional because soot are formed in a conical layer and transported through the flaming zone by large-scale dominated turbulence. Soot formation and depletion may change the magnitude of soot volume fractions of the streaks, but not their spatial distribution patterns. However, further investigations are needed to confirm this and the scale-up possibility. The magnitude of the instantaneous soot volume fractions increases from the fuel surface, reaches the peak value, and then decreases towards the flame tip. The maximum soot volume fraction in the instantaneous LII images typically appears at $H = 2D$ above the burner exit. The peak value of the instantaneous soot volume fractions in this turbulent flame is comparable to that in laminar flames [23]. These features can be utilized as criteria to evaluate soot models in fire simulations. The similarity between the laminar and turbulent flame soot streaks should be exploited in modeling turbulent fire.

3.2. Ensemble mean and the RMS in the methane flame

The averaged soot volume fractions at five downstream locations in the 7.1 cm methane flame are shown in Fig. 4. It can be seen that the averaged soot volume fraction distributions are qualitatively different from the instantaneous images shown in Fig. 2. The instantaneous streaky structures are completely smeared in the averaging process so that the mean distributions become much more axisymmetric. Because the flame is axisymmetric in the mean, the average soot volume fractions are centered on the burner axis within a one diameter cylindrical zone. The peak of mean soot volume fractions in the entire flame

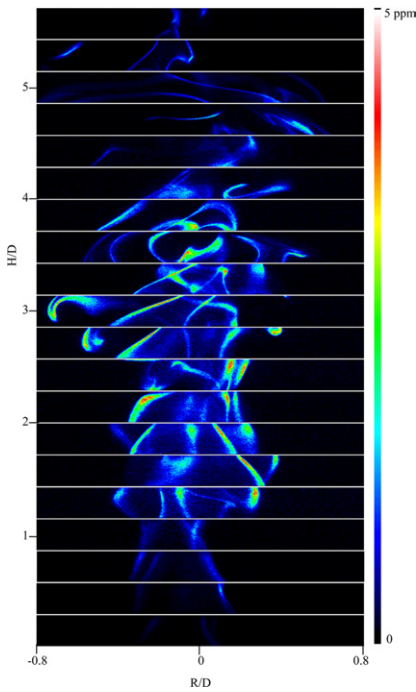


Fig. 2. Collage of instantaneous images of soot volume fractions in a 7.1 cm methane flame.

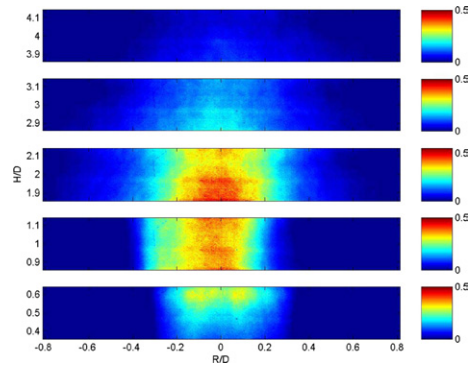


Fig. 4. Averaged soot volume fractions in a 7.1 cm methane flame. The color bar denotes ppm.

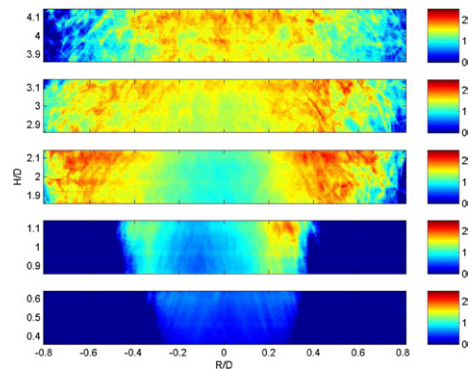


Fig. 5. Fluctuation intensities of soot volume fractions in a 7.1 cm methane flame.

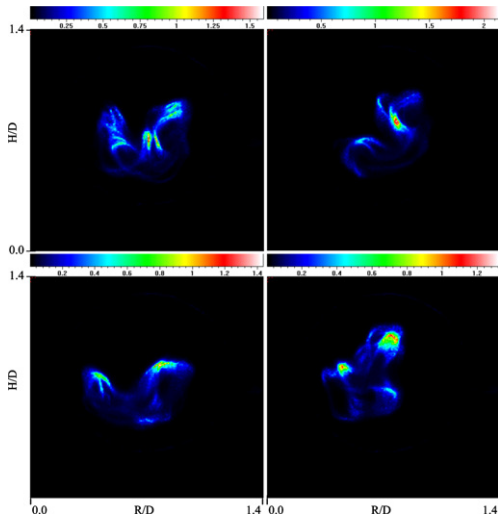


Fig. 3. Instantaneous horizontal soot images in a 7.1 cm methane flame at $H = 0.5D$. The color bar denotes arbitrary units.

is approximately an order of magnitude lower than the instantaneous value, which is largely because of the intermittency. The soot volume fractions increase with downstream distance up to $H = 2D$ (also see Fig. 2), then decrease toward

the flame tip, which signifies the competition between soot formation and oxidation along the downstream direction.

The soot fluctuation intensities—defined as the ratio of the RMS and the mean, are shown in Fig. 5. The peak intensities indicate that the soot volume fractions can fluctuate around the mean by more than a factor of 2. The spatial distributions of the fluctuation intensities vary substantially along downstream direction. In the lower elevations of $H = 0.5D, 1D,$ and $2D$, the high fluctuation intensities occur in an annular region. At the higher elevation where $H = 4D$, the region of high soot fluctuation intensities broadens to the entire flame volume. The fluctuation intensity distribution at $H = 3D$ is a transition between these two modes. Comparing Figs. 4 and 5, it is readily seen that the peak mean and peak fluctuation intensities of soot volume fractions are not spatially aligned with each other. This suggests that the intermittency effects are relatively weak in the regions where high soot volume fractions most probably exist.

3.3. PDF and SCC in the methane flame

The PDFs of soot volume fractions at different locations in the flame are shown in Fig. 6. For all locations except where $H = 1D$ and $R = 0D$, the most probable soot volume fractions exist below 0.5 ppm. Most of the PDF profiles except those at $R = 0D$ and $H = 1/2D, 1D$, and $2D$ are in log-normal shape with the peaks toward zero and the long tails toward high soot volume fractions. This suggests that soot volume fractions are most probably very low at these locations, but may exhibit very high values with a relatively small likelihood. At locations of $H = 0.5D, 1D$, and $2D$ along the burner axis ($R = 0D$), the PDFs of the soot volume fractions are dispersed over a relatively broad range in the sampling space. However, these broadening effects rapidly decrease along both radial and vertical directions.

SCC of the soot volume fractions is defined as $SCC = (\overline{f_v' f_v'}) / (\overline{f_v} \overline{f_v})$, where f_v is the soot volume fraction. The prime denotes fluctuation around the mean, and the subscripts θ and r denote the center of a probe region and a vector distance from the center. SCCs were computed based on 3500 samples at selected square regions centered at radial distance $R = 0D, 0.2D$, and $0.4D$ at five downstream locations (Fig. 7). At $H = 2D-4D$, the SCCs decrease rapidly from unity at the center of the correlation region to zero along radial and axial directions. At the lower elevations of $H = 0.5D$ and $1D$, the SCC decrease much slower along the axial direction compared to the radial direction. Very little soot was observed at the location of $R = 0.4D$ and $H = 0.5D$. Therefore, only self-correlation is seen in the lower-right panel in Fig. 7. These features suggest that the soot structures are organized over relative large vertical length scales near the flame base compared to those near the flame tip in the plume region, i.e., the isotropy of soot increase along downstream distance in such a buoyant tur-

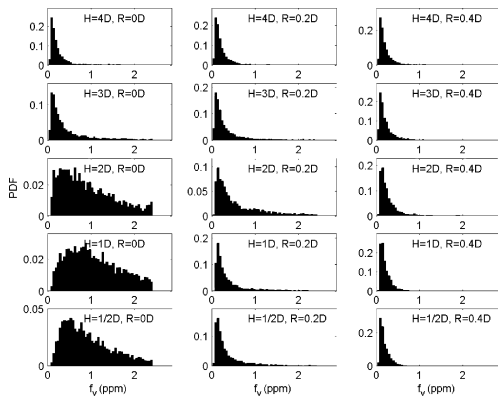


Fig. 6. PDF of soot volume fractions in a 7.1 cm methane flame.

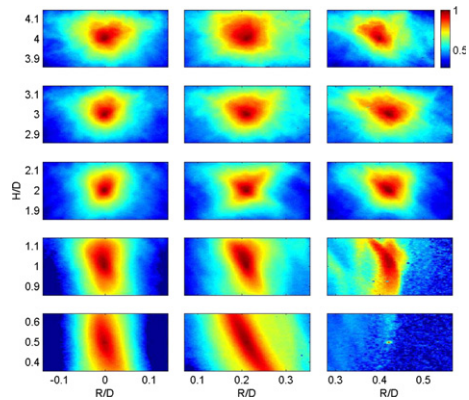


Fig. 7. SCC of soot volume fractions in a 7.1 cm methane flame.

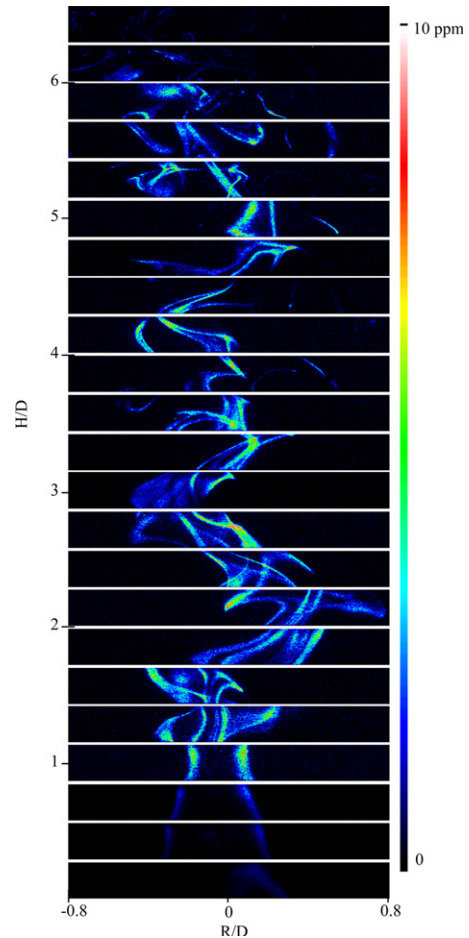


Fig. 8. Collage of instantaneous images of soot volume fractions in a 7.1 cm ethylene flame.

bulent fire. Comparing the instantaneous soot structures (Fig. 2) and the SCC (Fig. 7), it can be found that although the mean soot distributions

are quite homogeneous at higher elevations as a result of turbulent transport and high intermittency, the instantaneous soot structures are still streaky even in the regions where the flow is fully turbulent. Therefore, turbulence models capable of treating high levels of intermittency, departure from isotropy, and return to isotropy are necessary to capture soot behavior in buoyant fires.

3.4. Fuel effect

The soot volume fractions in methane flames are usually lower than those in other hydrocarbon flames. Therefore, the soot distributions in a 7.1 cm ethylene flame were measured to further examine the fuel effect. However, strong laser attenuation effect was observed in this flame, as mentioned before. Therefore, the results shown in this section reflect only the qualitatively differences between the two fuels.

A collage of the instantaneous soot volume fraction distributions in the 7.1 cm ethylene flame is shown in Fig. 8 analogous to Fig. 2. Comparison between these two figures confirms that the important features of instantaneous soot distributions observed in the methane flame are not sensitive to the fuel type. The only significant difference is the magnitude of the peak instantaneous soot volume fractions. More details on statistics of soot volume fractions in the ethylene flame, which show similar features as those of the methane flame, can be found in [24].

4. Conclusions

Spatially resolved two-dimensional soot volume fractions were measured using planar LII technique in turbulent buoyant flames fueled by methane and ethylene gases. Factors affecting LII signals including LEP and laser attenuation were considered. The absolute soot volume fractions were obtained by comparison to existing extinction measurements. Statistical quantities of the soot volume fraction including the ensemble average, RMS, PDF, and SCC were computed using instantaneous samples. The results show that:

- (1) In the entire flame, soot particles exist in streaks with an apparent thickness of 1–2 mm, which exhibit two-dimensional structure and occupy only a very small fraction of the flame zone. The soot streaks are anchored above the burner exit in the persistent zone, but wrinkled and twisted by the turbulent flow field in the intermittent and plume zones.
- (2) Ensemble averaged soot volume fractions increase with downstream distance from the burner exit, reach the peak values, and then decrease toward the flame tips. The intermit-

tency strongly affects the average so that the peak mean is about an order of magnitude lower than the instantaneous value.

- (3) High fluctuation intensities occur in an annular region by a factor of 2 around the mean. The peak mean and peak fluctuation intensity of soot volume fractions are not spatially aligned with each other in the persistent zone.
- (4) The PDFs are relatively homogeneous at the observed locations, but the spatial correlations of soot volume fractions are anisotropic. However, the isotropy increases along the downstream distance.
- (5) The soot distribution features observed above are qualitatively insensitive to fuel effect by comparison of methane and ethylene flames.

Acknowledgments

This work is supported by the National Institute of Standards and Technology under the Grant No. 60NANA9D0093 with Dr. Howard Baum and Dr. Anthony Hamins serving as NIST Scientific Officers.

References

- [1] A. Hamins, M. Klassen, J.P. Gore, T. Kashiwagi, *Combust. Flame* 86 (1991) 223.
- [2] A. Hamins, S. Fischer, T. Kashiwagi, M. Klassen, J.P. Gore, *Combust. Sci. Technol.* 97 (1994) 37.
- [3] M. Klassen, J.P. Gore, Y.R. Sivathanu, A. Hamins, T. Kashiwagi, *Proc. Combust. Inst.* 24 (1992) 1713.
- [4] M. Klassen, Y.R. Sivathanu, J.P. Gore, *Combust. Flame* 90 (1992) 34.
- [5] M. Klassen, J.P. Gore, *Combust. Flame* 93 (1993) 270.
- [6] K.B. McGrattan, H.R. Baum, R.G. Rehm, A. Hamins, G.P. Forney, Fire Dynamics Simulator—Technical References Guide, National Institute of Standards and Technology, Report No. NISTIR 6467 (2000).
- [7] K.B. McGrattan, H.R. Baum, R.G. Rehm, A. Hamins, G.P. Forney, J.E. Floyd, S. Hostikka, Fire Dynamics Simulator—Technical Reference Guide (Version 2), National Institute of Standards and Technology, Report No. NISTIR 6783 (2001).
- [8] J.P. Gore, G.M. Faeth, *Proc. Combust. Inst.* 21 (1986) 1521.
- [9] S. Leonardi, A Study of Radiation Heat Transfer of Porous Burner. Ph.D. thesis, Purdue University (2002).
- [10] A.C. Eckbreth, *J. Appl. Phys.* 48 (1977) 4473.
- [11] L.A. Melton, *Appl. Opt.* 23 (1984) 2201.
- [12] C.J. Dasch, *Appl. Opt.* 23 (1984) 2209.
- [13] C.R. Shaddix, K. Smyth, *Combust. Flames* 107 (1996) 418.
- [14] T. Ni, J.A. Pinson, S. Gupta, R.J. Santoro, *Appl. Opt.* 34 (1995) 7083.

- [15] R.L. Vander Wal, *Appl. Optics* 35 (1996) 6548.
 [16] B. Quay, T.W. Lee, T. Ni, R.J. Santoro, *Combust. Flames* 97 (1994) 384.
 [17] H. Zhao, N. Ladommatos, *Prog. Energy Combust. Sci.* 24 (1998) 221.
 [18] M.A. Delichatsios, *Combust. Flames* 70 (1987) 33.
 [19] X.C. Zhou, J.P. Gore, H.R. Baum, *Proc. Combust. Inst.* 28 (1996) 1453.
 [20] R.J. Santoro, C.R. Shaddix, Laser-induced incandescence, in: *Applied combustion diagnostics*, first ed., Taylor & Francis, London, 2003, pp. 252–286.
 [21] P. Joulain, *Proc. Combust. Inst.* 27 (1998) 2691.
 [22] H. Geitlinger, T. Streibel, R. Suntz, H. Bockhorn, *Proc. Combust. Inst.* 27 (1998) 1613.
 [23] C.S. McEnally, L.D. Pfefferle, *Proc. Combust. Inst.* 27 (1998) 1539.
 [24] Y. Xin, *A Theoretical and Experimental Study of Buoyant Turbulent Flames with Emphasis on Soot and Radiation*, Ph.D. thesis, Purdue University, 2002.

Comments

Gus J. Nathan, University of Adelaide, Australia.
 Could you please comment on the effects of attenuation on your measurement?

Reply. Two attenuation effects exist in our LII measurements: the attenuation of laser incidence along its propagation path and the attenuation of LII signals as observed by the ICCD. In the three fuels we studied, the strongest attenuation of laser was seen in the acetylene flames, while moderate and negligible laser attenuation was observed in the ethylene and methane flames, respectively. Therefore, the major portion of the paper reports the measurements in the methane flame. We selected 410 nm as the detection wavelength to minimize the attenuation of LII signals by the flame.

•

M.A. Mikofski, University of California-Berkeley, USA. Please describe how the LII measurement of f_v was calibrated.

Reply. Based on LII theory and practice [10–16], the LII signal is approximately proportional to f_v . Therefore, the absolute f_v values in turbulent fires were calibrated using past extinction measurements in a laminar

flame [8]. Because the f_v in the laminar flame is known and the LII signals can be measured using the same experimental system, we obtained a linear calibration constant. This constant was then applied to the measured LII signals in turbulent fires to convert the relative LII signals to absolute f_v values.

•

K. P. Geigle DLR Stuttgart, Germany. Concerning the PDFs showing a distribution at some point, and recognizing the very small sooting structure, there should be a lot of events with 0 ppm. How big is the region for which those PDFs are determined (single pixel—1 mm)?

Reply. It is true that a lot of events with very low soot volume fractions contribute to the PDF calculation. This is precisely the reason that we observed lognormal PDFs at many locations, which indicates that soot structures at these locations are highly intermittent. The PDFs were not computed in 2D regions, but for a single pixel in the probe plane, e.g., $H = 1$ D and $R = 0.2$ D. The spatial resolution of the receiving optics and the ICCD is 0.2×0.2 mm² per pixel, while the laser plane thickness is about 1 mm.